Mechanical characterisation and micromechanical modelling of bread dough

M. A. P Mohammed, E. Tarleton, M. N. Charalambides, J. G. Williams

Mechanical Engineering Department, Imperial College London, SW7 2AZ London, UK

Synopsis

The mechanical behaviour of dough, gluten and starch was studied in an effort to investigate whether bread dough can be treated as a two phase (starch and gluten) composite material. Mechanical loading tests revealed rate-dependent behaviour for both the starch and gluten constituents of dough. There is evidence from cryo-Scanning Electron Microscopy (SEM) that damage in the form of debonding between starch and gluten occurs when the sample is stretched. In addition, the Lodge material model was found to deviate from the tension and shear stress-strain test data by a considerably larger amount than from the compression test data. This could indicate that 'damage' is dominant along the gluten-starch interface, causing debonding; the latter occurs less under compression loading, but is more prevalent in tension and shear loading. A single-particle finite element model was developed using starch as a filler contained in a gluten matrix. The interface between starch and gluten was modelled using cohesive zone elements with damage/debonding occurring under opening/tension and sliding/shear modes. The numerical results are compared to experimental stress-strain data obtained at various loading conditions. A comparison of stress-strain curves obtained from 2D and 3D single-particle models and a multi-particle model led to good agreement, indicating that the single-particle model can be used to adequately represent the microstructure of the dough studied here.

I. INTRODUCTION

Baking performance and quality of the bread produced are strongly dependent on the mechanical behaviour of dough used. Two major components of wheat flour dough that are believed to influence the mechanical properties of dough are starch and gluten. On

applying mechanical action during mixing, hydrated gluten aggregates partially dissociate, unfold and stretch to form a gluten phase throughout the dough [Amemiya and Menjivar (1992)]. The starch granules and gluten phase then interact by forming starch-starch, starch-gluten or gluten-gluten interactions. Starch-starch and starch-gluten interactions are an important source of elasticity in the dough which is affected by the starch concentration present. The interactions store potential energy upon deformation and thus contribute to the elastic behaviour of dough. The stress-strain relationship for dough can be interpreted using these interactions, as illustrated in Fig. 1 for the simplest mode of deformation, uniaxial tension. The curve shown is one that was measured in the current work at a strain rate of 5/min. The starch and gluten interactions (1, 2 and 3 in Fig. 1(b)) can be divided into four regions; pre-yield, plateau, strain-hardening and post fracture corresponding to regions i to iv in Fig1(a) respectively.

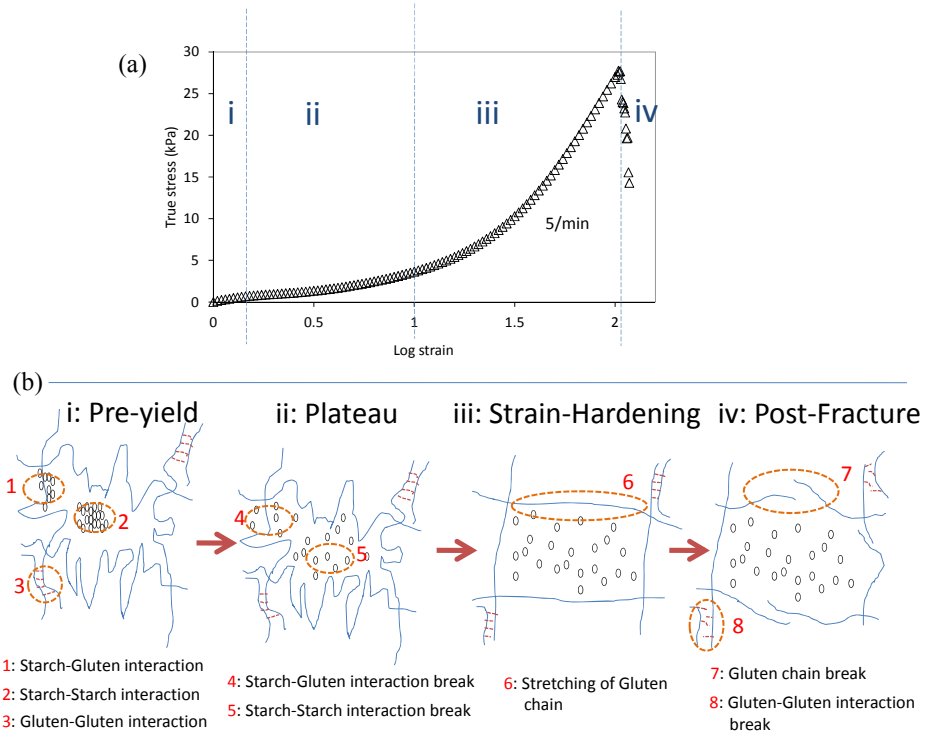


FIG. 1. (a) Stress-strain curve of wheat flour dough under uniaxial tension in different regions, and (b) starch and gluten interactions in the different regions ((b)i is reproduced from Amemiya and Menjivar (1992) and (b)iii from Dobraszczyk and Morgenstern (2003)). Stress and strain in 1(a) are calculated through Eqs. (1) and (2).

In the pre-yield region (region i in Fig. 1(a)), short range starch-starch and starch-gluten interactions are likely to dominate the response measured (1 and 2 in Fig. 1(b)) whilst gluten-gluten interactions (3) have a minor effect. In the plateau region (region ii in Fig. 1(a)), starch-starch and starch-gluten interactions start to break down due to deformation (4 and 5 in Fig. 1(b)). It is likely [Dobraszczyk and Morgenstern (2003)], based on the theory of polymer melts, that disentanglement in gluten-gluten interactions at some point may permit the gluten chain to move about freely and act as a viscous liquid. When the dough enters the strain hardening region (region iii in Fig. 1(a)), the microstructure is determined by two processes: further break down of short-range

interactions which cause flow, and resistance by longer-range gluten-gluten interactions (6 in Fig. 1(b)) [Amemiya and Menjivar (1992)]. When a continuous gluten phase is present, gluten-gluten interactions dominates the region and the continuous network gives rise to the strain hardening effect. This phenomenon is also known as elastomeric behaviour [Ferry (1980)]. Singh and MacRitchie also suggest that extension of large glutenin molecules in gluten gives rise to behaviour akin to rubber elasticity. Finally, in the post fracture region (region iv in Fig. 1(a)), the stress reaches a peak and the gluten chain and gluten-gluten interactions begin to break down (7 and 8 in Fig. 1(b)).

To model the stress-strain curve of dough based on the microstructure theory in Fig. 1 would be very complex due to the multiple interactions taking place in the various strain regimes. In this work, we concentrate on the starch-gluten interaction and its breakdown (4 in Fig. 1b) and therefore the analysis that follows is limited up to the end of region ii (plateau region) with maximum strains close to one. Our approach is based on a micromechanics model which considers dough as a composite material with two solid phases; a starch filler contained in a gluten matrix, where starch is stiffer than the matrix. However, it has been reported that at large strains, gluten exhibits a higher stress-strain curve than dough [Uthayakumaran *et al.* (2002)]. This is in contrast with the composite material theory, where in the case of a stiffer filler, the composite material is expected to be stiffer than the matrix alone. It is hypothesized that the reason for this is due to damage or debonding of the starch-gluten interface. In a weakly bound filler-matrix composite material, the filler-matrix interaction will start to damage and eventually debond at some value of energy release rate [Meddad and Fisa (1997)].

This work investigates the mechanical behaviour of dough, gluten and starch. The possibility of damage at the interface between the starch and gluten is investigated. This is performed by using a two phase (starch and gluten) composite material model and

comparing the model predictions to experimental stress-strain data for dough tested under various loading conditions.

II. MATERIALS & METHODS

Bread dough produced in industry normally consists of wheat flour, water, salt, yeast, emulsifier and sweetener. To provide a simpler mechanical/rheological study, only a simple mixture of wheat flour, salt and water is considered here. The flour used for all experiments is strong white bread flour purchased from Wessex Mill in Oxford, UK. The starch and gluten contents in the flour are 86.1 % and 13.9 % respectively, which were obtained from dough washing procedures described later in this work. A mixture of 198.5 g of wheat flour, 120 g of distilled water and 1.5 g of sodium chloride is used to make the dough. All samples were mixed for three minutes using an instrumented laboratory 6-pin mixer at a constant speed in ambient conditions. Three minutes was found to be the 'optimum' mixing time, i.e. the mixing torque reached a maximum at this time. Following mixing, dough is separated to smaller portions and wrapped using cling film. Paraffin oil is applied to maintain the moisture on the surface of the sample. The test environment is controlled at 50 % relative humidity and a temperature of 22 ^{0}C .

Starch and gluten were separated from the dough by washing the dough under running tap water to remove most of the starch granules. The sample was gently rubbed by hand to ensure that the starch was removed from the gluten matrix. The remaining water in the gluten was allowed to drip out by leaving the sample to rest for approximately 60 minutes on water absorbent paper. Gluten obtained using this method is also known as wet/native gluten. Wet/native gluten as opposed to vital gluten was used in this work because the gluten network formed during mixing of dough is still retained, which makes it possible to determine the properties of the gluten as it appears in the actual dough material [Ng (2007)].

A similar dough washing procedure was performed to collect the starch granules. Rather than draining the water containing starch during the washing of dough, it was collected in a steel tray. The starch/water solution was allowed to dry for approximately 24 hours at a temperature of 22 ^{0}C and 50 % relative humidity. The drying process was assisted by a fan. It was found that leaving the samples to dry for longer than 24 hours did not lead to significant further weight loss. In addition, the dried starch was not crushed into powdered starch to prevent damaging the starch granules.

The reconstituted wet starch was obtained by adding dry starch to a prescribed amount of water. The amount of water added to the starch needs to represent the starch water content in dough. Thus the water distribution between flour components, i.e. starch and gluten, needs to be known. Two methods are available to achieve this, namely the simple liquid addition method and the water vapour absorption method [Roman-Gutierrez *et al.* (2002a); (2002b)]. To choose between these methods requires information on the hydration properties of the flour components and Roman-Gutierrez *et al.* (2002b) discussed that this depends on two factors: 1) ability of the flour components to trap water molecules, and 2) their ability to trap large amounts of water inside macromolecular complexes formed by the swollen flour components. These factors are difficult to quantify due to the flour components (i.e. starch and gluten) competing for water during the hydration process [Ng (2007)]. This in turn makes it almost impossible to determine directly the water distribution for each flour component when water is added during mixing.

Therefore assumptions are made in the methods to determine the water distribution between the flour components. In the simple liquid addition method, the gluten is assumed to take the water first for hydration before the remaining water is then taken by starch. This method was initially attempted by measuring the weight of starch and gluten

obtained from the dough washing procedures. The weights of dried and wet gluten as well as dried starch were recorded, enabling the water distribution in each dough phase to be calculated as 52% (starch) and 48% (gluten). These corresponded to a water content (mass of water/ dry mass) of 0.35 and 2.15 for starch and gluten respectively. However it was found that the hydrated starch sample obtained using this formulation was very dry and powdery when moulded into a cylindrical shape for the compression tests. Under uniaxial compression, the starch was observed to crumble rather than uniformly deform.

The alternative was to use the water content data for dough and gluten reported by Roman-Gutierrez *et al.* (2002b). They used the water vapour absorption method and measured the ability of the individual flour components to trap water molecules, without considering any competing effects for water between the flour components. Their method involved measuring the mass of an initially dry sample, placed on an atmospheric microbalance in a continuous flow of air, at controlled relative humidity. The mass of water absorbed at different humidities was then used to determine the theoretical distribution of water in dough, through the Guggenheim-Anderson-de-Boer (GAB) model. The theoretical water distribution among flour components for a strong wheat flour was approximately 88 % for starch and 12 % for gluten/others at 60 % relative humidity and 25 ^{0}C. It is worth noting that the flour used in this work is also a strong wheat flour, similar to the one used by Roman-Gutierrez *et al.* (2002b). Therefore, their suggested water distribution values were used to estimate the water content of starch. These results are summarised in Table I. First the dry gluten weight was measured experimentally and is shown as 27.5 g in [1b], Table I ([1b] implying column [b], row [1]). This was then used to obtain the dry starch weight [1a] from the known weight of dry flour [1c]: i.e. [1a]=[1c]-[1b]. It should be noted that the value calculated in [1a] was found to be somewhat larger than the experimentally measured value (165 g). This may

be due to some starch being lost during the starch preparation procedure. The distribution of water in row [4] was taken from Roman-Gutierrez *et al.* (2002b) as already explained above. This enables the rest of the entries of the Table to be calculated.

TABLE I. Starch and gluten composition in dough using the water vapour absorption method.

	[a] Starch	+	**[b] Gluten**	=	**[c] Flour / Dough**
[1] Dry weight (g)	171		27.5		198.5
[2] Wet weight (g)	276.6		41.9		318.5
[3] Water content (g)	105.6		14.4		120
[4] Distribution of water (%)	88		12		100
[5] Water-content/Dry-weight	0.62		0.52		0.60

The starch sample obtained using the formulation in Table I contained a larger amount of water than the starch samples following the formulation determined from the simple liquid addition method. As a result, it was found that the starch from Table I formed a cohesive, paste-like substance which could easily be formed into compression test samples. Uniform deformation occurred during uniaxial compression, as shown in Fig. 2. Therefore it was decided that the formulation in Table I would be used for the mechanical tests of starch in this work.

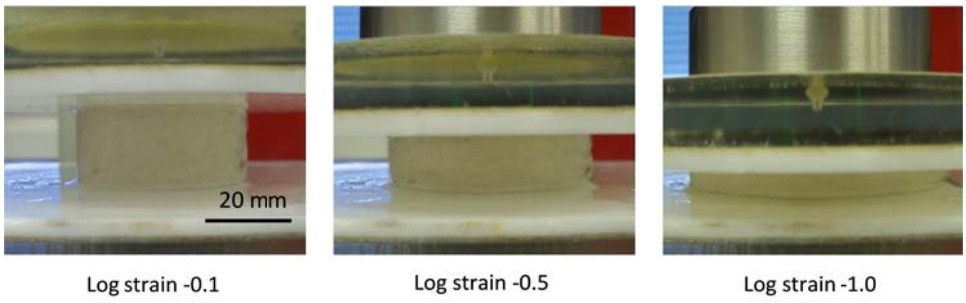


FIG. 2. Uniaxial compression results of starch at 5/min. Log strain is evaluated through Eq. (2).

The dough, wet gluten and reconstituted wet starch were formed into cylindrical samples of 40 mm diameter and 20 mm height for compression testing, and 6.8 mm diameter and 27 mm height for tensile testing [Charalambides *et al.* (2006)]. All samples were allowed to relax for 30 minutes before testing to allow residual stress in the samples to diminish. At least three replicate samples were tested for each loading condition to determine reproducibility.

The platens used in the compression tests were made from polytetrafluorethylene (PTFE) and had a diameter of 12 cm. In order to reduce friction further, silicon oil with a viscosity of 500 centistokes was applied on the loading surfaces. Charalambides *et al.* (2005) showed that under these conditions, the effect of friction on the compression data is largely eliminated and the resulting deformation is uniform. This allows accurate stress-strain data to be obtained.

Mechanical tests under compression and tension modes were performed using the Instron 5543 with 1 kN and 100 N load cells respectively. The tests were performed at constant strain rates as opposed to constant crosshead speeds. To keep the strain rate constant, the crosshead speed was set to decrease or increase exponentially with time for compression and tension, respectively. Under uniaxial compression and uniaxial tension modes, the corresponding values of load, P, and deflection, δ, were recorded. The true stress, σ, and log strain, ε, were calculated as:

$$\sigma = \frac{4Pl}{\pi D^2 l_0} \tag{1}$$

and:

$$\varepsilon = \ln \frac{l}{l_0} = \ln \lambda \tag{2}$$

where l_0 is the original height, D is the original diameter and l is the current height defined as $\left(l = l_0 + \delta\right)$, where deformation, δ, is defined in tension as $\delta > 0$ and $\delta < 0$ in compression. Note that Eq. (1) assumes a constant volume deformation and corrects the stress for the increase and decrease in cross sectional area during compression and tension respectively [Charalambides *et al.* (2002)].

Cyclic-compression tests were also performed. The sample is compressed and subsequently unloaded to zero stress at the same strain rate; subsequent reloading-unloading cycles followed at the same strain rate. An additional Teflon film of 25 μm thickness was positioned between the top, reversing platen and the sample as an extra precaution to ensure that zero tension is applied on the sample during the unloading phase of the test. An example of the applied log strain versus time plot for cyclic tests on gluten is shown in Fig. 3. Note that the sample was in contact with the platens throughout these tests.

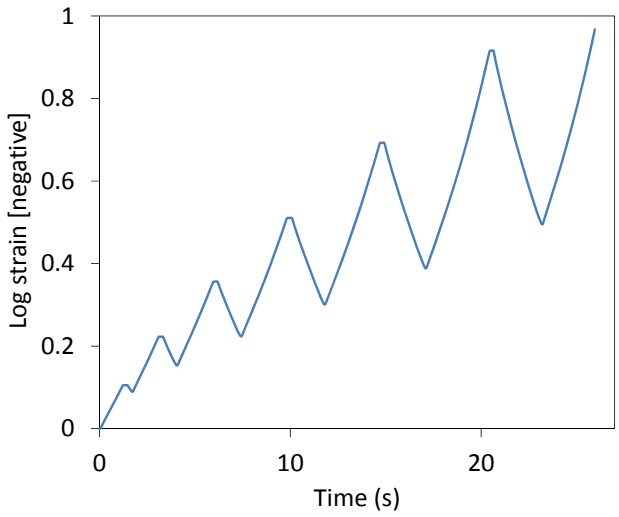


FIG. 3. Log strain vs time for cyclic-compression of gluten at 5/min.

Shear tests were performed using the rheometer model TA2000ex. The tests were conducted using a parallel plate configuration. The parallel plate geometry is preferable for soft solid samples [Macosko (1994)] as sand paper can be easily attached on the parallel plate surface [Ng (2007); Tanner *et al.* (2008)] to prevent slippage of the sample during the tests. For this work, sand paper of 100 grit size grade was used on a 40 mm diameter parallel plate geometry with a 3 mm gap. These test parameters were chosen according to suggestions by Keentok and Tanner (1982) who investigated shear stress using parallel plate and cone-plate geometries with different gap, H, values. They proposed a minimum gap size of 1 mm and (H/R) □ 0.05, beyond which the shear stress and normal stress in parallel plate geometry is unaffected by the gap, and good agreement was seen between the stress data from cone-plate and parallel plate geometries. Once the sample is loaded onto the rheometer, the excess dough at the side of the plates was removed using a sharp blade. A thin layer of silicon oil was then applied at the sides to prevent drying at the edges of the sample. The temperature of 22 ^{0}C at the rheometer base (Peltier plate) is controlled by a water circulating temperature control unit (Julabo AWC 100). The samples were allowed to relax for at least 30 minutes before the tests, to allow residual stress in the samples to diminish [Phan-Thien *et al.* (1998); Ng and McKinley (2008)].

In parallel plate geometry, the shear strain is a function of the radius, varying from zero at the centre of the sample, to a maximum at the edge of the rotating plate, *R*. The shear rate, $\dot{\gamma}_R$, at the edge of a parallel plate geometry is defined as:

$$\dot{\gamma}_R = \frac{R\omega}{H} \tag{3}$$

where ω is the rotational speed and H is the constant gap between the upper and lower rheometer plates. Tanner *et al.* (2008) have shown that edge fracture in dough samples occurs at a shear strain of approximately 20.

A last note regarding the shear data is the correction needed for the apparent rim shear stress calculated by the rheometer at large shear deformations as outlined by Ng *et al*. (2011) and Phan-Thien *et al.* (2000). The motivation for this correction is that at large strain, the material is non-linear and this might affect the accuracy of the rheometer calculations which assume a linear stress-strain relationship. The correction procedure outlined by Ng *et al.* (2011) was employed, i.e. the following equation was used to correct for the stress output from the rheometer, σ_R :

$$\sigma = \sigma_R \left[\frac{3}{4} + \frac{1}{4} \frac{\gamma_R}{\sigma_R} \frac{\mathrm{d}\sigma_R}{\mathrm{d}\gamma_R} \right] \tag{4}$$

where γ_R is the strain at the rim of the plate. This correction was found to be rather small, i.e. the Root Mean Square Percentage Error (RMSPE) was in the order of 6 % for gluten and 16 % for dough.

Finally, the cryo-SEM test equipment (model ALTO 2100) manufactured by Gatan was used in the cryo-SEM tests. The tests were performed on dough and gluten samples mixed from the same batch. The dough samples were stretched and compressed manually just before exposure to liquid nitrogen, such that a comparison could be made with images of unstretched samples. All specimens were slushed in liquid nitrogen under vacuum conditions before being transferred to the cryo chamber; they were freeze-fractured, sublimated at -90 ^{0}C for 2 minutes and gold-sputtered before being imaged in the SEM chamber.

III. LODGE RUBBERLIKE MODEL FOR BREAD DOUGH

Dough has been shown to behave like a critical gel by various researchers [Gabriele *et al.* (2001); Ng *et al.* (2006); Lefebvre (2006); Migliori and Gabriele (2010); Tanner *et al.* (2008); (2011a)]. A critical gel material can be modelled using the Lodge rubberlike model [Lodge (1964)], based on the study by Winter and Chambon (1986) and Winter and Mours (1997). The Lodge model is described as:

$$\boldsymbol{\sigma} + p\mathbf{I} = \int_{-\infty}^{t} \frac{d}{dt'}\left[G\left(t - t'\right)\right]\mathbf{C}^{-1}\left(t, t'\right)dt' \tag{5}$$

where $\boldsymbol{\sigma}$ is the stress tensor, p is the pressure, $\mathbf{I}$ is the unit tensor, G is the relaxation function, and the Finger deformation tensor $\mathbf{C}^{-1}\left(t, t'\right)$ is described with respect to the present time, t. A power law for the function G was considered in Tanner *et al.* (2008) as shown below:

$$\boldsymbol{\sigma} + p\mathbf{I} = \int_{-\infty}^{t} \frac{d}{dt'}\left[G(1)\left(t - t'\right)^{-n}\right]\mathbf{C}^{-1}\left(t, t'\right)dt' \tag{6}$$

where:

$$G\left(t\right) = G(1)t^{-n} \tag{7}$$

[Migliori and Gabriele (2010); Ng and McKinley (2008)]. Therefore, Eq. (6) becomes:

$$\boldsymbol{\sigma} + p\mathbf{I} = \int_{-\infty}^{t} nG(1)\left(t - t'\right)^{-(n+1)}\mathbf{C}^{-1}\left(t, t'\right)dt'. \tag{8}$$

The Lodge rubberlike model can be used to predict data from various mechanical tests. The Finger tensor $\mathbf{C}^{-1}\left(t, t'\right)$ is evaluated for the different loading conditions, i.e.

tension, compression and shear. Under uniaxial tension, the Lodge model can be approximated by [Ng and McKinley (2008)]:

$$\sigma_{zz} - \sigma_{rr} \approx \sigma \approx G(1)\dot{\varepsilon}^{n}\varepsilon^{-n}\left(\exp(2\varepsilon) + \frac{(1+2n)}{1-n}\varepsilon - 1\right) \tag{9}$$

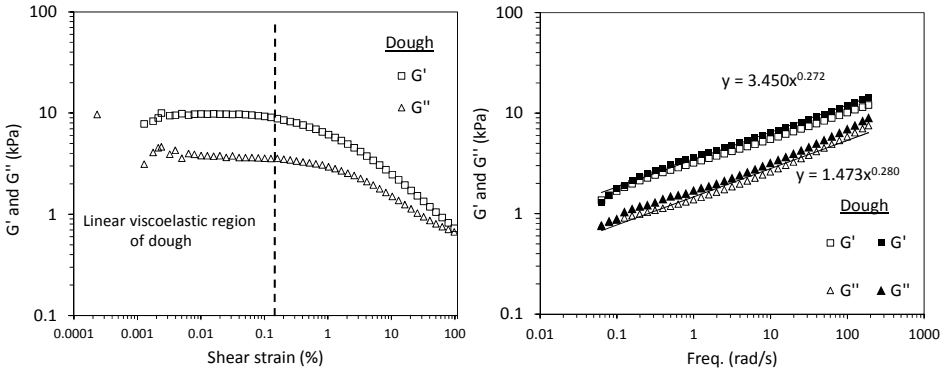
where $\dot{\varepsilon}$ is strain rate and ε is log or Hencky strain. σ_{zz} and σ_{rr} are referred to as the axial and radial stresses of a cylindrical specimen respectively. Another approximation to the Lodge model solution under uniaxial tension was suggested by Tanner *et al.* (2008) and was compared to Eq. (9). The results from the two approximations were found to be almost identical (results not shown). Also note that Eq. (9) is used for uniaxial compression loading too, where a negative strain is used to indicate compressive strain.

From Eq. (6), the shear stress, σ, under simple shear loading is expressed as [Tanner *et al.* (2008); Ng and McKinley (2008)]:

$$\sigma = \frac{G(1)\dot{\gamma}^{n}}{1-n}\gamma^{1-n}. \tag{10}$$

The stress relaxation constant, $G(1)$ and power law constant, n, are determined from small amplitude oscillatory shear (SAOS) tests (i.e. strain sweep and frequency sweep tests), following the procedures in Tanner *et al.* (2008) and Ng and McKinley (2008). The strain sweep tests were performed at 1 Hz and the results are shown in Fig. 4(a). It is observed that strain amplitude of 0.1 % is within the linear viscoelastic region of dough. The frequency sweep tests were therefore performed at 0.1-30 Hz and 0.1 % strain. The data are shown in Fig. 4(b). The storage and loss moduli plots are each approximated with a power law such that:

$$G'(t) = G'(1)\omega^n, \quad G''(t) = G''(1)\omega^n \tag{11}$$



(a) (b)

FIG. 4. SAOS test results of dough: (a) strain sweep tests in the shear strain range of up to 100 % at 1 Hz, and (b) frequency sweep at 0.1 % shear strain at 0.1-30 Hz.

Therefore the power law constant, n, was obtained from the average of the two exponents shown in Fig. 4(b), where $n \approx 0.27$. This value was used to calculate $G(1)$ using the following relationship [Tanner *et al.* (2008)]:

$$G(1) = G'(1)\frac{2(n!)}{n\pi}\sin\frac{n\pi}{2} \tag{12}$$

where $n!$ is the factorial function of the power law constant, which is equal to $\Gamma(n+1) = 0.902$ for $n = 0.27$, and $G'(1)$ is equal to 3.45 kPa/(rad/s)$^{0.27}$, as shown in Fig. 4(b). Thus $G(1)$ is calculated as 3.02 kPa s$^{0.27}$.

Fig. 5 shows the fit of the Lodge model to the dough test data under large deformation. The model leads to considerably higher stress values than the tension and shear test data, therefore suggesting the use of a damping function [Ng *et al.* (2006)] or a damage function [Tanner *et al.* (2008); (2011a)]. In contrast, the model is closer to the

compression test data, indicating that possibly less damage occurs under compression. In order to quantify the 'damage factor', the ratio of the experimental value to the Lodge model calculation is plotted against log strain, as shown in Fig. 5(d). Absolute/positive true stress and log strain are used for uniaxial compression, whereas the log strain for the shear tests is calculated using [Treloar (1975)]:

$$\varepsilon = \ln(\lambda) = \ln\left(\frac{\gamma}{2} + \frac{\sqrt{\gamma^2 + 4}}{2}\right) \tag{13}$$

A lower value of the experimental over Lodge model ratio indicates that a larger damage factor is needed in order to replicate the test results. It can be seen that the ratio for shear is the lowest followed by tension and compression. This suggests that debonding at the starch-gluten interface is possibly an important damage mechanism in dough. This can readily occur under shear and tension. During compression, debonding only arises from shear generated off-axis at 45° from the direction of the applied load, therefore the damage factor has lower values than in tension or shear loading.

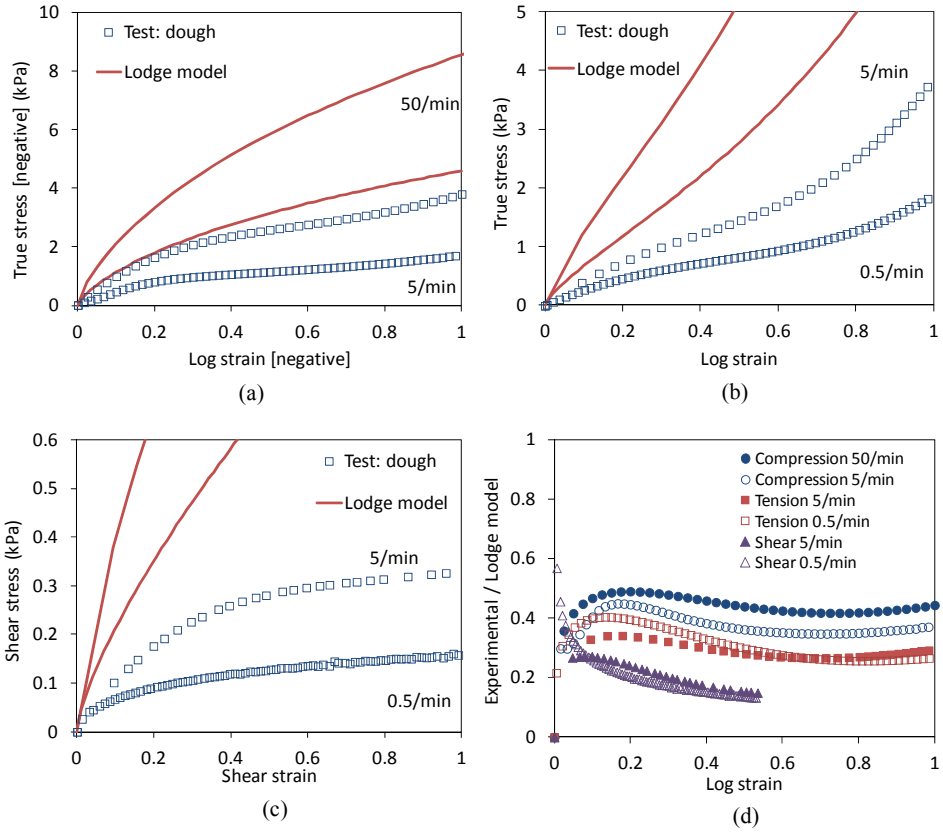


FIG. 5. Dough test data at 5/min and Lodge rubberlike model fit results under: (a) compression, (b) tension, (c) shear, and (d) Experimental over Lodge model ratio under different modes of deformation.

IV. MICROMECHANICS MODEL FOR BREAD DOUGH UNDER LARGE DEFORMATION

A. Cryo-SEM of bread dough

The results from the cryo-SEM tests are shown in Fig. 6. The starch appears as discrete large ellipsoidal or smaller spherical granules embedded in the gluten matrix. No starch granules are observed on the surface of the gluten sample, as shown in Fig. 6(b). The small holes in the gluten (i.e. in Fig. 6(a) and Fig. 6(b)) are artefacts due to evaporation of water during the sublimation process. Evidence of debonding at the starch-gluten

interface is observed for the stretched sample (Fig. 6(d)), such debonding was not present in the original sample (Fig. 6(a)). This suggests that the dough may be undergoing damage [Ng *et al.* (2006); Tanner *et al.* (2008)] due to the starch-gluten interaction weakening at large deformations. It is worth noting that debonding is less apparent when the dough was subjected to a compressive load (Fig. 6(c)).

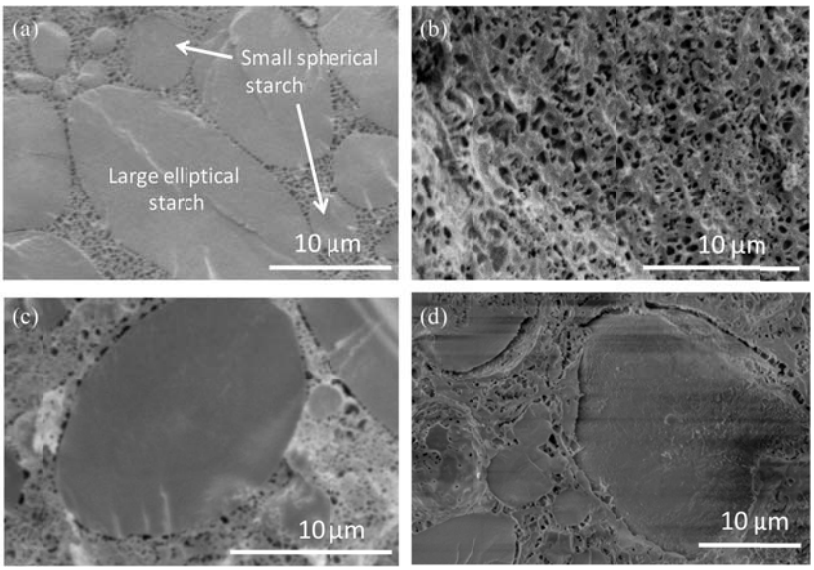


FIG. 6. Cryo-SEM images of: (a) undeformed dough, (b) undeformed gluten, (c) compressed dough, and (d) stretched dough.

B. Material model for gluten

The results from the mechanical tests on gluten are shown in Fig. 7. Gluten shows rate-dependent behaviour under compression, tension and shear modes, and energy dissipation under a cyclic-compression mode. The stress under constant applied strain is seen to relax over time under compression relaxation and shear relaxation modes. Noise is observed at times less than 3 seconds under small shear strain (shear strain of 0.1 % and 1%). The results indicate a rubberlike and strain-dependent material behaviour.

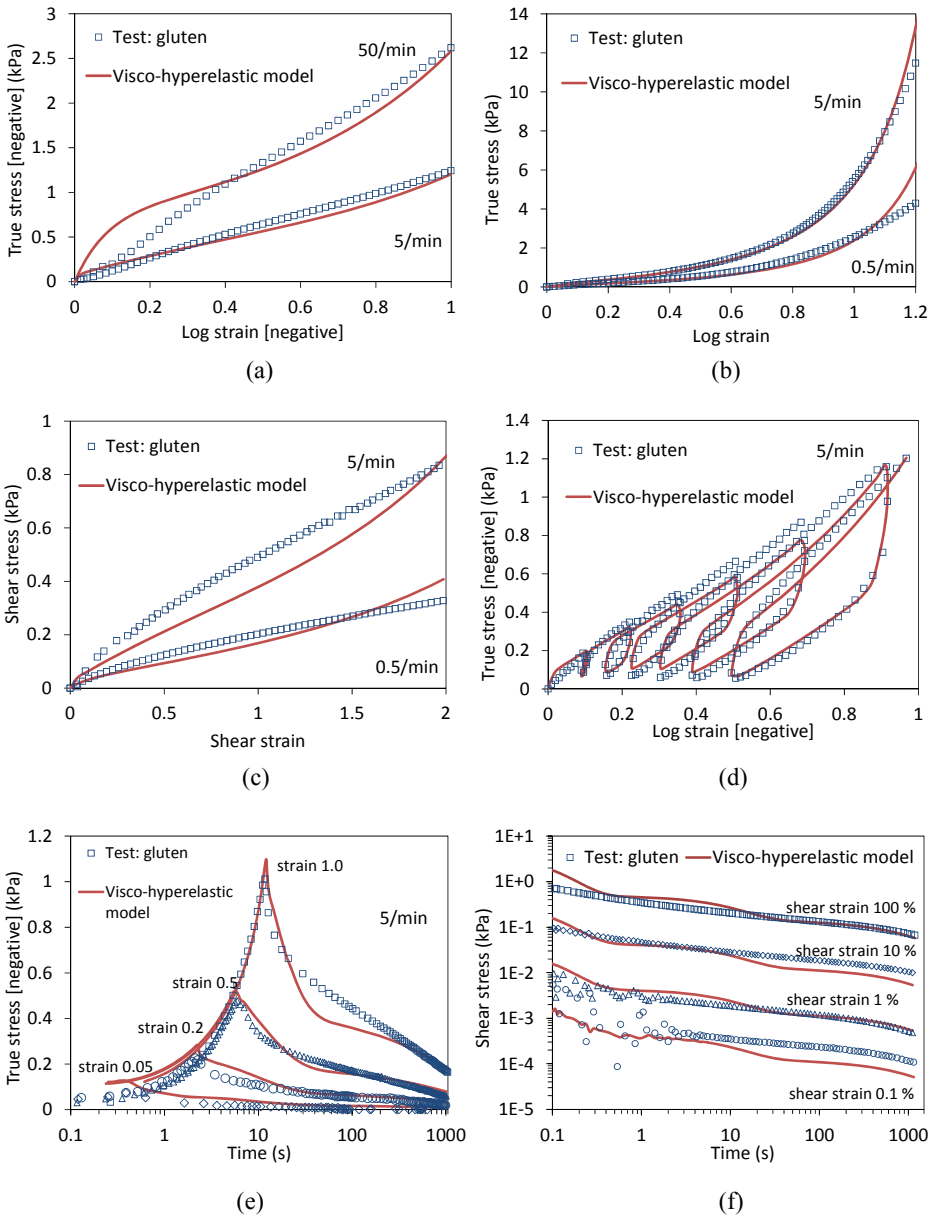


FIG. 7. Gluten test results and calibration of visco-hyperelastic (van der Waals) material model under: (a) compression, (b) tension, (c) shear, (d) cyclic-compression, (e) compression-relaxation, and (f) shear-relaxation. The model is described by Eq. (14) to Eq. (19).

Material parameters of gluten under large deformation were determined using a visco-hyperelastic material model, where the van der Waals strain energy function and the

Prony series time-dependent function were used. Assuming a homogeneous and isotropic material, for separable time- and strain-dependent material behaviour [Goh *et al.* (2004); Charalambides *et al.* (2006)], the relaxation stress under a step strain loading history can be written as a product of a function of time, $g(t)$, and a function of strain, $\sigma_0(\varepsilon)$:

$$\sigma(\varepsilon,t) = \sigma_0(\varepsilon)\, g(t). \tag{14}$$

The time function is represented by the Prony series [Goh *et al.* (2004)]:

$$g(t) = g_\infty + \sum_{i=1}^{N} g_i \exp\left(-\frac{t}{\xi_i}\right) \tag{15}$$

where t and ξ_i are time and time constants respectively, and g_i are dimensionless constants related to g_∞ through $\sum_{i=1}^{N} g_i + g_\infty = 1$. For an arbitrary strain history, the stress can be described using the Leaderman form of convolution integral [Williams (1980)]:

$$\sigma(\varepsilon,t) = \int_0^t g(t-s)\frac{d\sigma_0(\varepsilon)}{ds}ds \tag{16}$$

where $\sigma_0(\varepsilon)$ is the instantaneous stress at strain ε. In this work, the van der Waals model is used as the hyperelastic potential [Kilian (1980); Kilian and Vilgis (1984); Enderle and Kilian (1987); Vilgis (1992)] for the function $\sigma_0(\varepsilon)$. The true stress form for uniaxial tension and uniaxial compression can be described using $\sigma_0(\lambda) = \frac{\partial W}{\partial \lambda}\lambda$, where W is the hyperelastic potential and λ is the stretch ratio (see Eq. (2)). The stress for uniaxial tension and uniaxial compression, $\sigma_0(\varepsilon)$, can then be derived as:

$$\sigma_0(\lambda)=\mu\lambda\left(\lambda-\frac{1}{\lambda^2}\right)\left[\frac{\sqrt{\lambda_m^2-3}}{\sqrt{\lambda_m^2-3}-\sqrt{\lambda^2+2\lambda^{-1}-3}}-a\sqrt{\frac{\lambda^2+2\lambda^{-1}-3}{2}}\right] \tag{17}$$

where μ is the instantaneous initial shear modulus, λ_m is the locking stretch constant and a is the global interaction parameter [Abaqus (2009)].

For simple shear loading, shear stress, $\sigma(\lambda)$, can be written using the chain rule as: $\sigma(\lambda)=\frac{dW}{d\gamma}=\frac{dW}{d\lambda}\frac{d\lambda}{d\gamma}$, where λ is related to the shear strain γ through Eq. (13). The shear stress for simple shear is therefore derived as:

$$\sigma_0=\sigma(\lambda)=\mu\left(\frac{\lambda^3-\lambda^{-1}}{\lambda^2+1}\right)\left[\frac{\sqrt{\lambda_m^2-3}}{\sqrt{\lambda_m^2-3}-\sqrt{\lambda^2+\lambda^{-2}-2}}-a\sqrt{\frac{\lambda^2+\lambda^{-2}-2}{2}}\right]. \tag{18}$$

By substituting Eq. (15) in Eq. (14), and evaluating the integral using finite time increments [Taylor *et al.* (1970); Kaliske and Rothert (1997)], the following form is obtained:

$$\begin{aligned}\sigma(t_{n+1})&=g_\infty\sigma_0(t_{n+1})\\&+\sum_{i=1}^{N}\left(\exp\left(-\frac{\Delta t}{\xi_i}\right)h_i(t_n)+g_i\frac{1-\exp\left(-\frac{\Delta t}{\xi_i}\right)}{\frac{\Delta t}{\xi_i}}\left[\sigma_0(t_{n+1})-\sigma_0(t_n)\right]\right).\end{aligned} \tag{19}$$

Eq. (19) is a function for updating the stress $\sigma(t_{n+1})$ where Δt is the time step defined as $\Delta t=t_{n+1}-t_n$ and $h_i(t_n)=\int_0^{t_n}g_i\exp\left(-\frac{t_n-s}{\xi_i}\right)\frac{d\sigma_0(s)}{ds}ds$. A detailed derivation is given in Goh *et al.* (2004). The function can be evaluated for various strain histories.

The visco-hyperelastic model described above was calibrated using the gluten test data in Fig. 7. The calibration was performed simultaneously using a least squares method [Goh *et al.* (2004); Charalambides *et al.* (2006)]. A constraint was defined during the calibration procedure where the time-dependent constants, g_i, are set to be between 0 and 1. The parameters for the model are shown in Table II. The model agrees reasonably well with the gluten test data (RMSPE = 24 %), as shown in Fig. 7, justifying the assumption of the rubberlike, rate-dependent behaviour of gluten.

TABLE II. Visco-hyperelastic model parameters for gluten.

Material	**Strain-dependent constants**			**Time-dependent constants**					
				i	1	2	3	4	∞
	μ (kPa)	λ_m	a	ξ_i (s)	0.1	10	100	1000	
Gluten	3.29	4.64	0.25	g_i	0.867	0.092	0.004	0.028	0.007

It is worth noting here that methods have been suggested by Ng and McKinley (2008) and Tanner *et al.* (2011a) to derive the discrete Prony series terms from the power law fit to relaxation or storage modulus data (Eq. (6)). Such a method was attempted in this work with data from SAOS tests on gluten (data not shown). It was found that the resulting Prony Series terms did not lead to a good fit to the experimental data of Fig. 7 and therefore this method was not investigated further.

C. Material model for starch

Fig. 8 shows the results from the compression and compression-relaxation experiments on starch. Only compression test results are shown for starch. This is due to difficulties in preparing samples for tensile tests. In addition it was found that the starch

samples showed edge fractures during shear at small strains which led to irreproducible results.

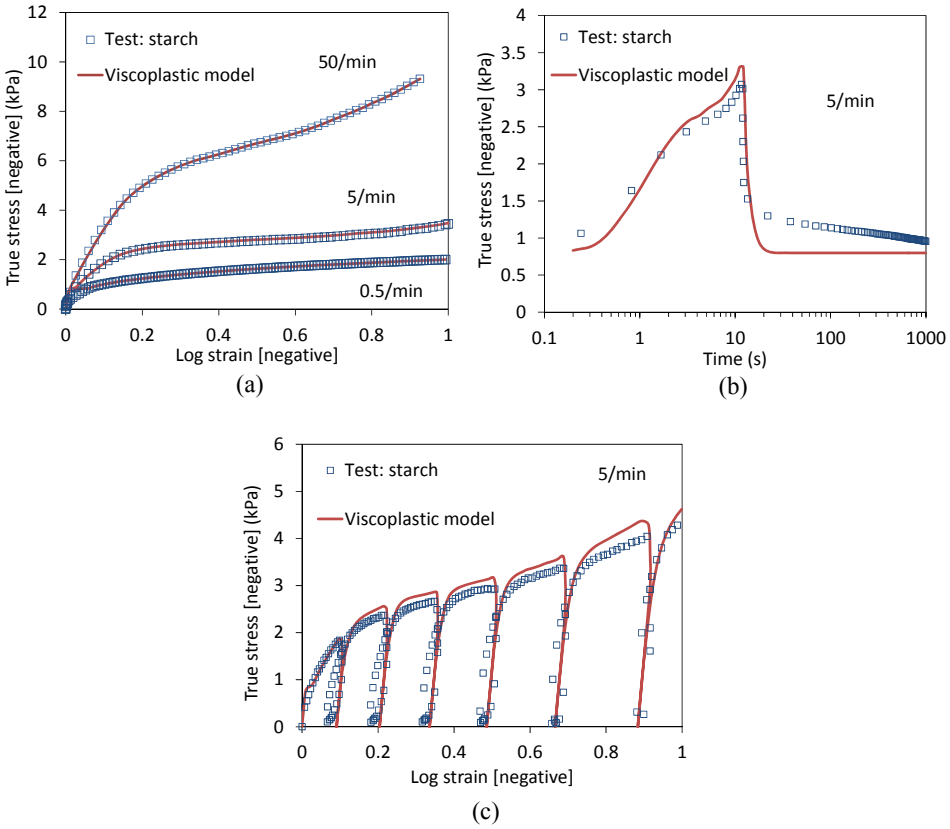


FIG. 8. Starch tests results and calibration of visco-hyperelastic material model with starch tests data under: (a) compression, (b) compression-relaxation at strain of 1, and (c) cyclic-compression.

The starch test results in Fig. 8(a) show a rate-dependent behaviour, which is similar to the results from gluten shown in Fig. 8. However, the almost vertical unloading-reloading parts of the cyclic results for starch (Fig. 8(c)) as well as the less dramatic relaxation (Fig. 8(b)), when compared to gluten results in Fig. 7, indicate viscoplastic behaviour. Therefore, a viscoplastic material model was considered to represent the mechanical behaviour of starch. In the Finite Element Analysis software Abaqus (2009), which was used for the micromechanics model in the following section, viscoplasticity

can be implemented through a strain rate-dependent yield behaviour which follows an initial elastic region. The software allows a direct tabular entry of corresponding equivalent stress and equivalent plastic strain test data at different plastic strain rates. The plastic strain is calculated through:

$$\varepsilon_{plastic}^{n} = \varepsilon_{total}^{n} - \varepsilon_{elastic}^{n} = \varepsilon_{total}^{n} - \frac{\sigma^{n}}{E} \tag{20}$$

where $\varepsilon_{plastic}^{n}$, ε_{total}^{n} $\varepsilon_{elastic}^{n}$ and σ^{n} are the plastic log strain, total log strain, elastic log strain and true stress respectively at the n^{th} experimental data point in the 'yield regions' of Fig. 8(a). Plastic strain rates are calculated in a similar fashion. The initial yield stress, $\sigma_{y} = 0.8$ kPa is selected to fit the stress relaxation data after 100 seconds (Fig. 8(b)). The elastic modulus, $E = 90$ kPa , on the other hand is estimated through the initial, almost linear, steep section of the unloading-reloading data in Fig. 8(c). Lastly, the Poisson's ratio, ν, is taken to be 0.49 assuming an incompressible material [Charalambides *et al.* (2002); Wang *et al.* (2006)].The viscoplastic model is in reasonable agreement with the starch test data shown in Fig. 8.

D. Micromechanics model for dough

A simple composite model was developed using Abaqus [Abaqus (2009)], using a single-particle model, which consisted of a single 2D circular filler representing starch surrounded by matrix representing the gluten phase, as shown in Fig. 9(c). Gluten and starch were modelled through the visco-hyperelastic and the viscoplastic models shown in Figs. 7 and 8 respectively. The diameter of the filler is set to 20 μm , which is of the same order as the size of starch in dough as seen in Fig. 6. An average starch volume fraction value of 45 % was calculated from cryo-SEM images of dough. This is performed by converting the cryo-SEM image of dough to binary form using the image

analysis toolbox in MATLAB [MATLAB (2009)], with an example shown in Fig. 9(a) and Fig. 9(b).

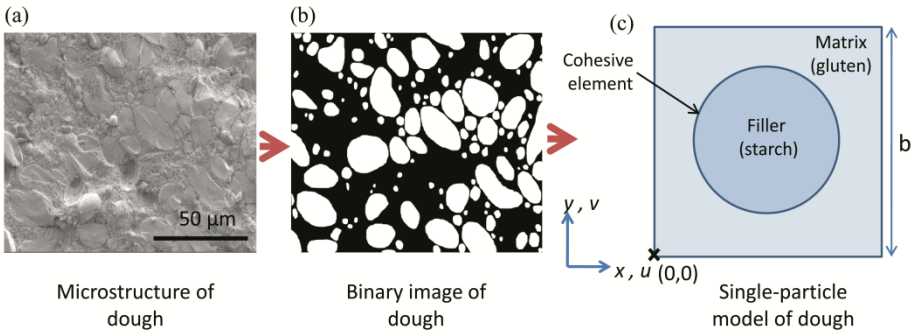


FIG. 9. Volume fraction measurement of dough: (a) cryo-SEM image of dough, (b) binary image of dough, and (c) a single-particle model of dough.

The black pixels in Fig. 9(b) represent the gluten matrix and the white pixels represent the starch granules. The starch volume fraction was determined from the ratio of the black and white pixels, i.e. the assumption that the 2D areal and 3D volume fractions are equal was made [Underwood (1970)]. The starch volume fraction obtained from images taken from the Cryo-SEM experiments is $45\,\% \pm 3\,\%$. The value is close to the 46 % starch volume fraction obtained in Tanner *et al.* (2011b).

The single-particle model was loaded uniaxially as well as in simple shear mode. The analysis was performed using Abaqus/Explicit [Abaqus (2009)] with linear, plane stress elements. In an attempt to simulate as close to 3D as possible, generalised plane strain elements were also considered. These however led to results very close to plane stress (results not shown) so plane stress elements were used throughout. The mesh density was chosen following a mesh sensitivity study where the mesh was refined sequentially until the numerical results converged to within $\pm 1\,\%$. Under tension and compression modes, the following boundary conditions were used:

$$u(0,0) = v(x,0) = 0$$

$$v(x,b) = \delta \tag{21}$$

where δ the applied displacement is $\delta > 0$ in tension and $\delta < 0$ in compression, u and v are displacements in the *x* and *y* direction respectively, *b* is the height of the single-particle model, and $(0,0)$ is the origin coordinate at the lower left corner of the single particle model, as shown in Fig. 9(c). Under simple shear, the following boundary conditions were used:

$$u(x,0) = v(x,0) = 0$$

$$u(x,b) = \delta\,;\, v(x,b) = 0. \tag{22}$$

Periodic boundary conditions were added for the model to undergo similar displacements on the vertical sides of the geometry in Fig. 9(c). However it was found that a very similar stress-strain curve was obtained when a comparison was performed between the results obtained with and without periodic boundary conditions (typical difference between results □ 0.5 %, results not shown). This indicates that the boundary conditions in Eq. (21) and Eq. (22) are sufficient for the single particle model. Finally, the output strain and strain rate ranges in all the simulations were checked to ensure that they lied within the strain and strain rate calibration ranges shown in Figs. 7 and 8.

The numerical results when no debonding/damage is allowed at the starch/gluten interface are first shown in Fig. 10 for the rate of 5/min. It is observed that the numerical predictions are close to the experimental stress-strain curves of dough for strains up to approximately 0.2 in compression and tension and 0.4 in shear loading. This gives further confidence that the constituents of dough, i.e. starch and gluten have been modelled

correctly. For higher strains, the experimental data are lower for all loading conditions. Even though shear and normal displacements coexist during shear and tensile loading of the micromechanics model, the comparison is still useful as it helps to form an approximate estimate of the critical stresses for the initiation of debonding damage; approximately 0.3 kPa in shear and 1.0 kPa in tension.

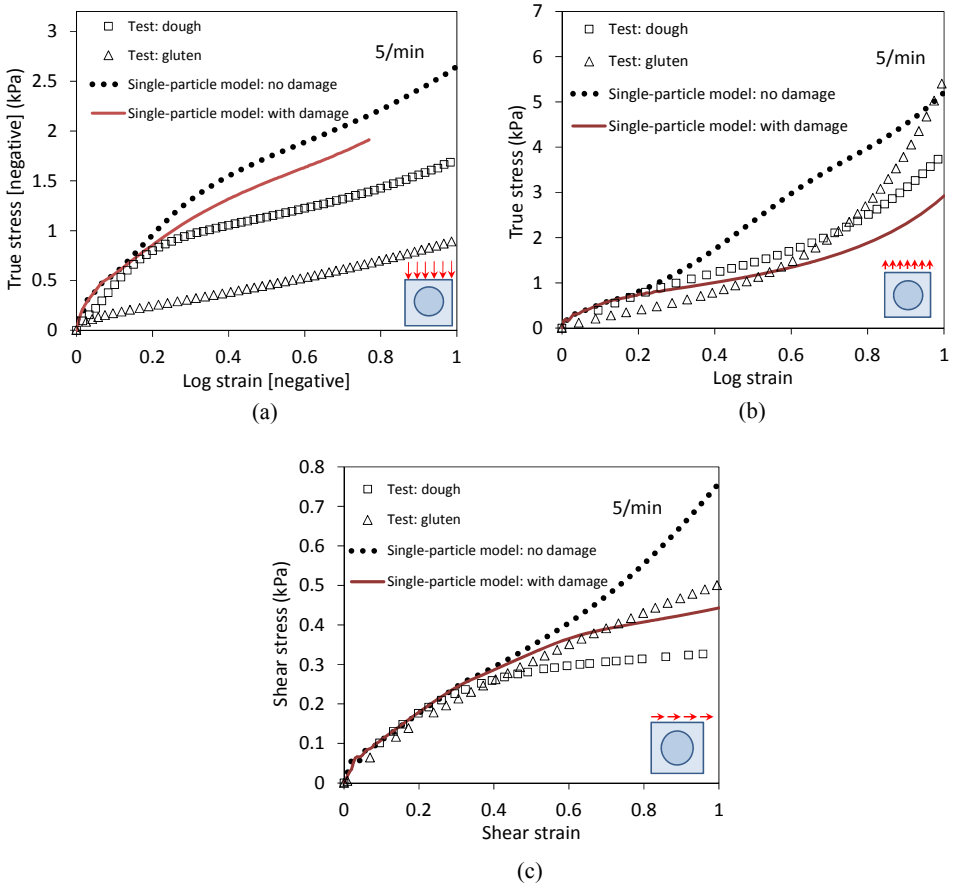


FIG. 10. Dough tests data at 5/min and calibration of the single-particle model under: (a) compression, (b) tension, and (c) shear.

Next, the interface between starch and gluten in Fig. 9(c) was modelled using the cohesive element interaction available in Abaqus [Camanho and Davila (2002)]. The

interaction is defined by the traction versus separation behaviour, which can be separated into two regions (see Fig. 11).

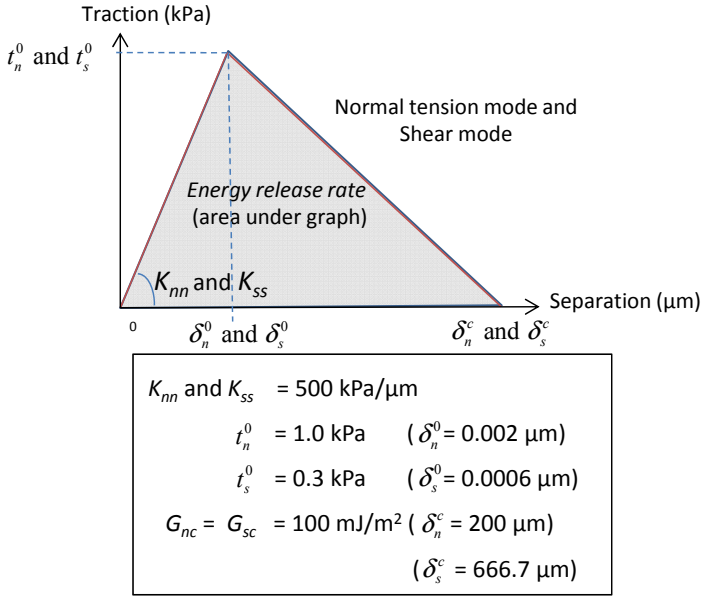


FIG. 11. Cohesive contact parameters used in the micromechanics model under normal and shear loading.

In the first region, the traction-separation is linear elastic and is described as:

$$\mathbf{t} = \mathbf{K}\boldsymbol{\delta} \quad \text{or} \quad \begin{Bmatrix} t_n \\ t_s \end{Bmatrix} = \begin{bmatrix} K_{nn} & 0 \\ 0 & K_{ss} \end{bmatrix} \begin{Bmatrix} \delta_n \\ \delta_s \end{Bmatrix} \tag{23}$$

where $\mathbf{t}$ is the nominal traction stress as a function of coefficient tensor, $\mathbf{K}$, and separation vector, $\boldsymbol{\delta}$. K_{nn} and K_{ss} are the normal and shear coefficients respectively. At the critical normal stress, t_n^0 or critical shear stress, t_s^0, damage initiates. Damage is activated in the normal and shear loading modes, in terms of a maximum stress criterion expressed as:

$$\max\left\{\frac{\langle t_n \rangle}{t_n^0}, \frac{t_s}{t_s^0}\right\} = 1 \tag{24}$$

where the symbol $\langle t_n \rangle$ represents the Macaulay bracket, defined as $\langle t_n \rangle = \frac{1}{2}\left(|t_n| + t_n\right)$, implying that damage is not initiated in compression. Progressive damage in the interface occurs until complete failure. The damage evolution law describes the rate at which the cohesive stiffness is degraded after the damage initiation criterion is reached. The energy that is dissipated as a result of the damage process, i.e. the energy release rate, G_c, is equal to the area under the traction-separation curve in Fig. 11, i.e. $G_{nc} = \frac{t_n^0 \delta_n^c}{2}$ and $G_{sc} = \frac{t_s^0 \delta_s^c}{2}$ for pure normal and shear loading conditions respectively. For mixed mode loading conditions which do arise at the interface of the circular particles, we assumed a linear mixed mode failure locus with the total energy release rate, *G*, being equal to:

$$G = G_n + G_s \qquad \text{and} \qquad \frac{G_n}{G_{nc}} + \frac{G_s}{G_{sc}} = 1 \tag{25}$$

where G_n and G_s are the energy release rates in the normal and shear directions.

Having already made estimates for t_n^0 and t_s^0 as 1.0 kPa and 0.3 kPa respectively, the values of G_{nc}, G_{sc}, K_{nn} and K_{ss} need to be next determined. In the absence of direct experimental data, the simplifying assumption that $G_{nc} = G_{sc}$ and $K_{nn} = K_{ss}$ is first made. The value of $K_{nn} = K_{ss} =$ 500 kPa/μm is then selected to reduce severe mesh distortion of the cohesive elements during the large strain simulations. This is because the values of K_{nn} and K_{ss} must be high enough to prevent interpenetration of the element faces and to prevent artificial compliance from being introduced into the model by the

cohesive elements [Song *et al.* (2008)]. The damage energy, $G_{nc} = G_{sc}$ = 100 mJ/m^2 is next obtained from peel tests of dough from a steel substrate performed by Dobraszczyk (1997). These parameters were used to predict the dough response under all loading conditions and the results are compared to experimental data in Fig. 10.

For tension and shear loading, when the interaction of starch and gluten is strong, as indicated for the dough with no damage, the stress-strain curve is above the gluten stress-strain curve under tension and shear. When damage is activated, the interface softens and debonds, causing the dough stress-strain curves under tension and shear to cross over the curves for gluten, leading to lower stress values than in gluten. This observation explains the trends in data published by other researchers [Uthayakumaran *et al.* (2002); Ng (2007)]. In contrast, damage is less apparent under compression and the stress-strain curve for dough is always higher than gluten.

The model predictions for the full range of loading conditions are shown in Fig. 12. The correct trends are predicted. For compression at 5/min and 50/min the errors are RMSPE = 25.5 % and RMSPE = 17.7 % respectively. Note that the simulations for compression aborted before the strain of one was reached due to large mesh distortion. The cyclic compressive loading shows good agreement to the test data. For tension at 5/min and 0.5/min, the errors are RMSPE = 18.8 % and RMSPE = 8.8 % respectively. The error for 5/min shear loading is RMSPE = 20.3 %. The errors are very large for shear at 0.5/min (RMSPE = 71.2 %). A probable reason is that the cohesive zone parameters could be rate-dependent [Geiβler and Kaliske (2010)].

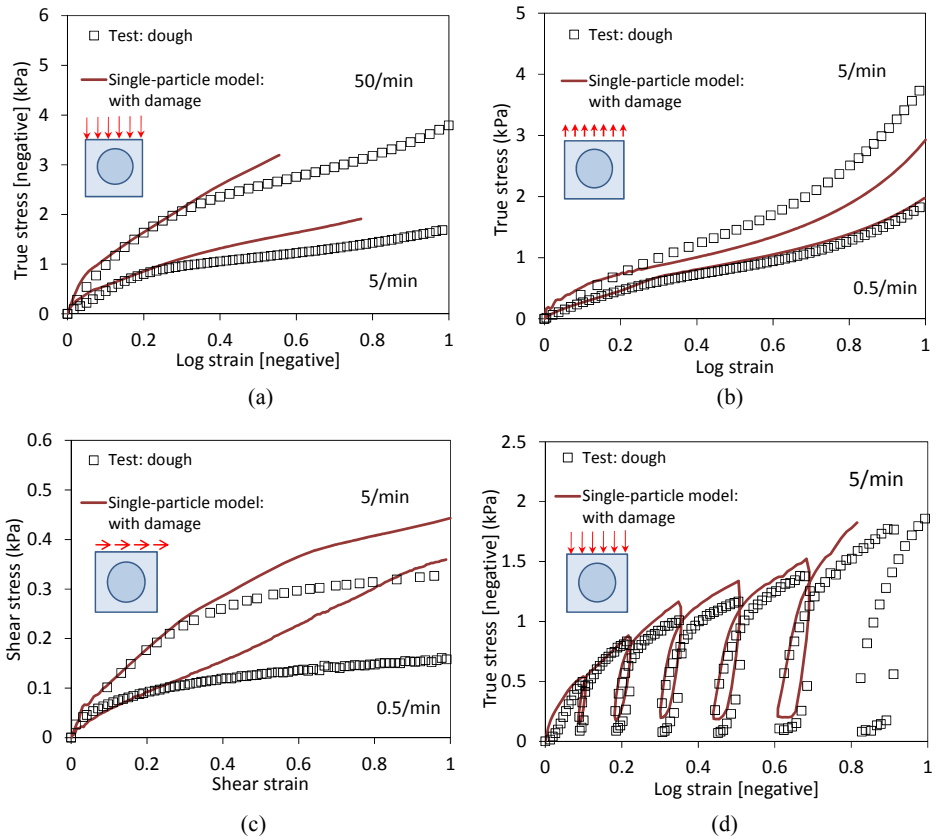


FIG. 12. Dough tests data and calibration of the single-particle model under: (a) compression, (b) tension, (c) shear, and (d) cyclic-compression.

In order to check the rate dependence possibility, Fig. 13 shows the numerical curve for shear loading at 0.5/min with no debonding allowed. By comparing this curve with the experimental data, it is apparent that debonding occurs at a stress of approximately 0.1 kPa which is a great deal lower than the assumed value of 0.3 kPa in Fig. 12. Indeed, when the critical shear stress is reduced to 0.1 kPa, the numerical curve is very close to the experimental data as shown in Fig. 13. However, implementing cohesive zone parameters as a function of rate requires thorough, direct, experimental measurement and justification. Suitable experiments could involve a single starch granule being pressed on a gluten surface and subsequently retracted, possibly through an Atomic Force

Microscope as is performed in synthetic polymer characterisation [Haupt et al. (1999)]. Such a task for the case of starch/gluten interface would be quite complex though, taking into account the nature of these soft, difficult to handle materials.

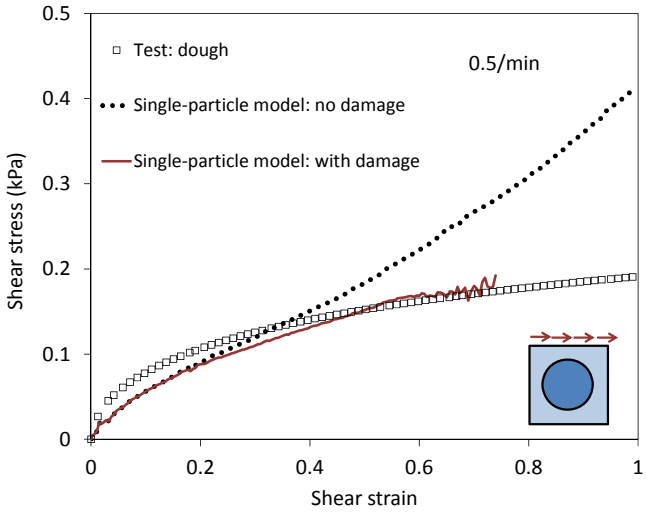


FIG. 13. Dough shear tests data at 0.5/min and calibration of the single-particle model using lower shear stress initiation value of 0.1 kPa. The other parameters for the single-particle model with damage are the same as in Fig. 11.

As already mentioned, the value of $G_{nc} = G_{sc}$ = 100 mJ/m^2 used in Fig. 11, was obtained from peel tests of dough performed by Dobraszczyk (1997). Those peel tests were performed to measure the 'stickiness' of dough on a steel plate, whereas in dough, the surface energy should be that of the starch and the gluten interface. Blancher *et al.* (2005) on the other hand obtained the free surface energy of dry flour using the contact angle measurement as $50\,\mathrm{mJ/m^2}$.

Following the above remark, as well as for investigating the 'uniqueness' of the set of cohesive parameters that were selected above (see Fig 11), it was decided to perform another simulation with a set of parameters such that $G_{nc} = G_{sc}$ were set to $50\,\mathrm{mJ/m^2}$. The values of the other two parameters which led to a good agreement with the tensile

data at 5/min were t_n^0 = 2 kPa and t_s^0 = 0.2 kPa. The results from this set of parameters are shown in Fig. 14 together with the experimental data as well as the numerical result corresponding to the earlier set of cohesive parameters (Fig. 11). Even though the parameters are different, the global results are very close. Therefore, the usual problem in inverse parameter identification is demonstrated, that of non-uniqueness. In order to solve this problem, direct experimental identification of the cohesive parameters is required as already suggested above.

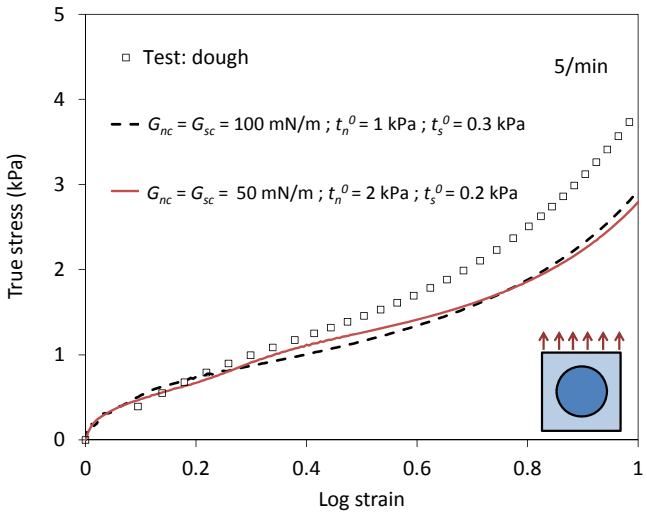


FIG. 14. The effect of two different sets of values for the cohesive parameters on global results under uniaxial tension.

In all simulations above, it was indicated that the critical shear stress for damage initiation is significantly lower than the critical normal stress. This implies that in Eq. (24), the condition for damage initiation will be largely determined by the shear critical stress for mixed mode loading. Therefore, it seems that the shear critical stress is a very important parameter for dough and its mechanical behaviour.

In order to investigate whether the single-particle model in Fig. 9(c) actually represents the microstructure of dough in Fig. 9(b), a comparison between the single-particle model and a multi-particle model with the same volume fraction was performed. The multi-particle model was developed by converting the binary image in Fig. 9(b) into a set of polygons representing the particles. This was achieved by using an algorithm based on the pixel connectivity to identify the particle boundaries which can then be approximated by a set of polygons [Tarleton, et al 2012]. The coordinates of the polygon vertices were then exported into Abaqus using a Python script to generate a mesh, as shown in Fig. 15(a). Cohesive elements were assigned along the interface of every particle and the same cohesive law and material models as used in the single particle model were applied. Simulation of the multi-particle model was conducted in Abaqus/Explicit using plane stress elements. Strains of up to 0.6 could be simulated under uniaxial tension, as shown in Fig. 15(b). The results under uniaxial tension obtained with the single particle model and the multi-particle model consisting of 141 particles are compared in Fig. 15(b), where a good agreement is observed. Simulations were also performed in compression and simple shear (results not shown). In compression the multi particle model could simulate strains up to 0.1 and the predicted response was in agreement with the single particle model; mesh distortion prevented larger strain compression simulations. In simple shear, the multi-particle and single particle models were found to agree for true strains up to 0.2; for larger strains the multi-particle model predicted a more compliant response (approximately 15% more compliant). The good agreement between the models, indicates that the single-particle model can be used to accurately represent the microstructure of dough.

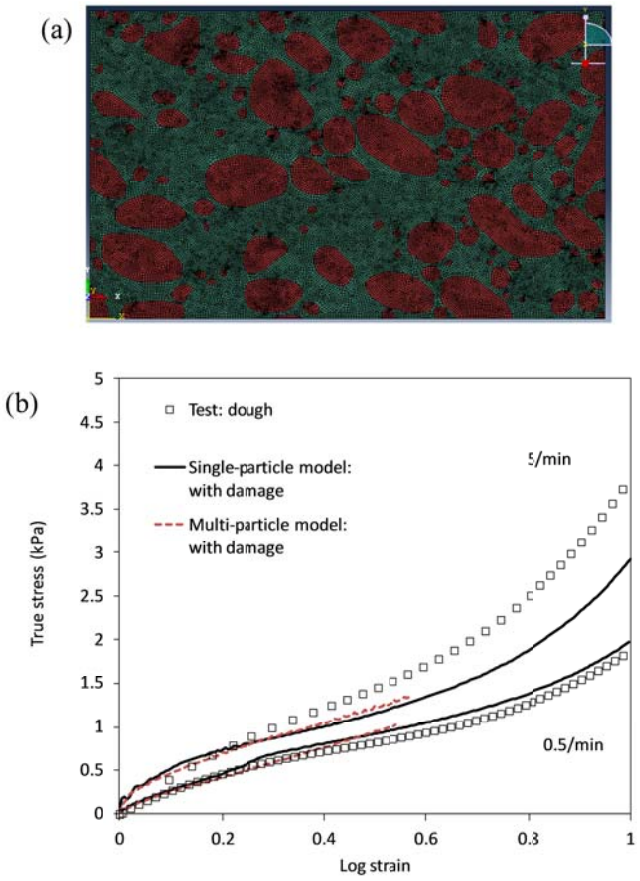


FIG. 15. (a) Multi-particle finite element mesh produced using the image in Fig. 9(b), and (b) comparison results between the single-particle model and the multi-particle model under uniaxial tension mode. The cohesive parameters used are as shown in Fig. 11.

A comparison was also performed between the 2D single-particle model and 3D single-particle models using spherical and cylindrical geometries. The same volume fraction, material models and cohesive law as used in the 2D single particle model were applied. The simulation results at 5/min under uniaxial tension are shown in Fig. 16. Reasonable agreement is observed between all the models, a further proof that the simple, 2D, single-particle model is sufficiently accurate for use in predictive models for the mechanical behaviour of dough.

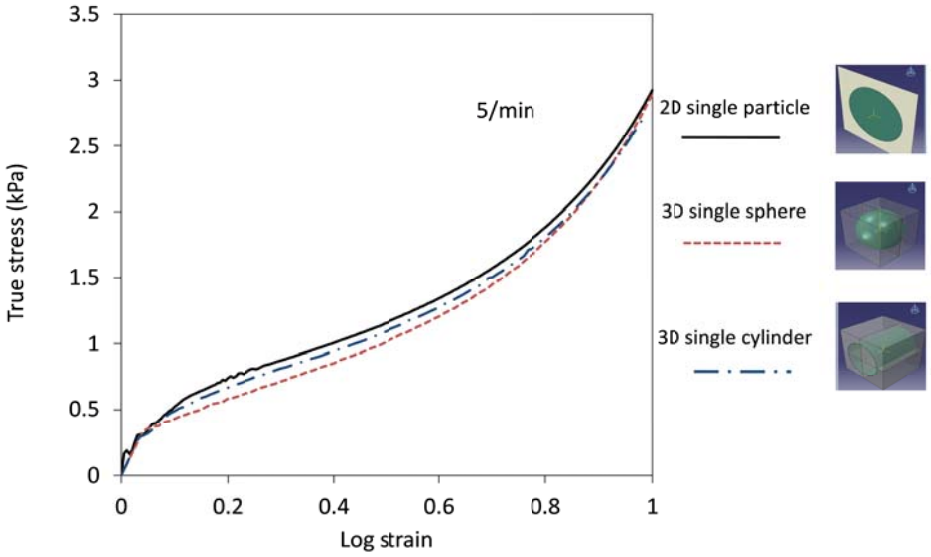


FIG. 16. Comparison results between the 2D single-particle and 3D single-particle models under uniaxial tension mode.

V. CONCLUSIONS

Mechanical loading tests were performed on starch, gluten and dough, which revealed rate-dependent behaviour for both the starch and gluten constituents of dough. A starch volume fraction of 45 % was measured experimentally from cryo-SEM images. Starch and gluten were modelled as visco-hyperelastic and viscoplastic materials respectively. A single-particle model was developed, which consists of a single 2D round filler representing starch surrounded by gluten matrix. The interaction between the starch and gluten was represented using cohesive elements. The simple composite model leads to similar trends as those shown by the experimental data, indicating possible debonding of starch and gluten in dough under tension and shear. This argument was supported further by cryo-SEM images of stretched dough as well as the apparent need for larger damage functions when the Lodge constitutive model was used to represent the mechanical test data of dough. Good agreement is seen between single-particle and multi-particle models,

as well as with 3D single-particle models with spherical and cylindrical geometries, indicating that the 2D single-particle model can be used to accurately represent the microstructure of dough. Finally, a direct experimental identification of the cohesive zone parameters is needed in order to identify the values for the critical damage initiation stress as well for the critical energy release rate in both normal and shear deformations as a function of test rate. Only then can numerical models such as the ones presented here can be fully validated against experimental data. However, the small size of starch particles and soft nature of the interface renders such tests a considerable challenge.

ACKNOWLEDGEMENTS

Financial support for this work is provided by the Malaysian Ministry of Higher Education and Universiti Putra Malaysia. The Cryo-SEM test equipment was purchased through funds from the EPSRC. Abaqus was provided under academic licence by HKS Inc., Providence, Rhode Island, USA. The authors would like to thank Prof. Roger Tanner from University of Sydney for helpful discussions.

References

Abaqus's user manual ver. 6.8 (Hibbitt Karlsson and Sorensen, Providence, 2009).

Amemiya, J. I., and J. A. Menjivar, "Comparison of small and large deformation measurements to characterize the rheology of wheat flour doughs," J. Food Eng. **16**, 91-108 (1992).

Blancher, G., M. H. Morel, E. Gastaldi, and B. Cuq, "Determination of surface tension properties of wheat endosperms, wheat flours and wheat glutens," Cereal Chem. **82**(2), 158-165 (2005).

Camanho, P. P., and C. G. Davila, "Mixed-mode decohesion finite elements for the simulation of delamination in composite materials," NASA/TM-2002-211737, 1-37 (2002).

Charalambides, M. N., L. Wanigasooriya, J. G. Williams, and S. Chakrabarti, "Biaxial deformation of dough using bubble inflation technique. 1. Experimental," Rheol. Acta **41**, 532-540 (2002).

Charalambides, M. N., S. M. Goh, L. Wanigasooriya, and J. G. Williams, "Effect of friction on uniaxial compression of bread dough," J. Mater. Sci. **40**, 3375-3381 (2005).

Charalambides, M. N., L. Wanigasooriya, J. G. Williams, S. M. Goh, and S. Chakrabarti, "Large deformation extensional rheology of bread dough," Rheol. Acta **46**, 239-248 (2006).

Dobraszczyk, B. J., "The rheological basis of dough stickiness," J. Texture Stud. **28**, 139-162 (1997).

Dobraszczyk, B. J., and M. P. Morgenstern, "Rheology and breadmaking process," J. Cereal Sci. **38**, 229-245 (2003).

Enderle, H. F., and H. G. Kilian, "General deformation modes of a van der Waals network," Prog. Colloid & Polym. Sci. **75**, 55-61 (1987).

Ferry, J. D., *Viscoelastic Properties of Polymers* (John Wiley and Sons, New York, 1980).

Gabriele, D., B. de Cindio, and P. D'Antona, "A weak gel model for foods," Rheol. Acta **40**, 120-127 (2001).

Gamonpilas, C., M. N. Charalambides, J. G. Williams, P. J. Dooling, and S. R. Gibbon, "Predicting the mechanical behaviour of starch gels through inverse analysis of indentation data," Appl. Rheol. **20**, 33283 (2010).

Geiβler G., and M. Kaliske, "Time-dependent cohesive zone modelling for discrete fracture simulation," Eng. Frac. Mech., **77**(1): 153-169 (2010).

Goh, S. M., M. N. Charalambides, and J. G. Williams, "Determination of the constitutive constants of non-linear viscoelastic materials," Mech. Time-Depend. Mater. **8**, 255-268 (2004).

Haupt, B. J., J. Ennis, and E. M. Sevick, "The detachment of a polymer chain from a weakly adsorbing surface using an AFM tip," Langmuir, **15**, 3886-3892 (1999).

Kaliske, M. and H. Rothert, "Formulation and implementation of three dimensional viscoelasticity at small and finite strains," Comput. Mech. **19**, 228-239 (1997).

Keentok, M., and R. I. Tanner, "Cone-plate and parallel plate rheometry of some polymer solutions," J. Rheol. **26**(3), 301-311 (1982).

Kilian, H. G., "A molecular interpretation of the parameters of the van der Waals equation of state for real network," Polym. Bull. **3**, 151-158 (1980).

Kilian, H. G., and T. H. Vilgis, "Fundamental aspect of rubber elasticity in real networks," Colloid and Polym. Sci. **262**, 15-21 (1984).

Lefebvre, J., "An outline of the non-linear viscoelastic behaviour in wheat flour dough in shear," Rheol. Acta **45**, 525-538 (2006).

Lodge, A. S., *Elastic Liquids* (Academic Press, New York, 1964).

Macosko, C. W., *Rheology: Principles, Measurements, and Applications* (John Wiley and Sons, New York, 1994).

MATLAB ver. 7.8 (The MathWorks Inc., Natick, 2009).

Meddad, A., and B. Fisa, "A model for filler-matrix debonding in glass-bead filled viscoelastic polymers," J. Appl. Polym. Sci. **65**, 2013-2024 (1997).

Migliori, M., and D. Gabriele, "Effect of pentosan addition on dough rheological properties," Food Res. Int. **43**, 2315-2320 (2010).

Ng, T. S. K., M. Padmanabhan, and G. H. McKinley, "Linear to non-linear rheology of wheat flour-water doughs," Appl. Rheol. **16**, 265-274 (2006).

Ng, T. S. K., "Linear to nonlinear rheology of bread dough and its constituents," Ph.D thesis, Massachusetts Institute of Technology, USA (2007).

Ng, T. S. K., and G. H. McKinley, "Power law gels at finite strains: the nonlinear rheology of gluten gels," J. Rheol. **52**(2), 417-449 (2008).

Ng, T. S. K., G. H. McKinley, and R. H. Ewoldt, "Large amplitude oscillatory shear flow of gluten dough: A model power law gel," J. Rheol. **55**(3), 627-654 (2011).

Phan-Thien, N., and M. Safari-Ardi, "Linear viscoelastic properties of flour-water doughs at different water concentrations," J. Non-Newton. Fluid Mech. **74**, 137-150 (1998).

Phan-Thien, N., M Newberry,and R.I. Tanner, "Non-linear oscillatory flow of a soft solid-like viscoelastic material," J. Non-Newton. Fluid Mech. **92**, 67-80 (2000).

Roman-Gutierrez, A. D., S. Guilbert, and B. Cuq, "Frozen and unfrozen water contents of wheat flours and their components," Cereal Chem. **79**(4), 471-475 (2002a).

Roman-Gutierrez, A. D., S. Guilbert, and B. Cuq, "Distribution of water between wheat flour components: A dynamic water vapour adsorption study," J. Cereal Sci. **36**, 347-355 (2002b).

Singh, H. and F. MacRitchie, F., "Application of Polymer Science to Properties of Gluten", J. Cereal Sci. **33,** 231–243 (2001).

Song, K., C. G. Davila, and C. A. Rose, "Guidelines and parameter selection for the simulation of progressive delamination," Abaqus User's Conference, Newport, Rhode Island, 1-15 (2008).

Tanner, R. I., *Engineering Rheology* (Oxford University Press, New York, 2000).

Tanner, R. I., F. Qi, and S. C. Dai, "Bread dough rheology and recoil: 2. Recoil and relaxation," J. Non-Newton. Fluid Mech. **143**, 107-119 (2007).

Tanner, R. I., S. C. Dai, and F. Qi, "Bread dough rheology and recoil: 1. Rheology," J. Non-Newton. Fluid Mech. **148**, 33-40 (2008).

Tanner, R. I., F. Qi, and S. Dai, "Bread dough rheology: An improved damage function model," Rheol. Acta **50**, 75-86 (2011a).

Tanner, R. I., S. Uthayakumaran, F. Qi, and S. Dai, "A suspension model of the linear viscoelasticity of gluten doughs," J. Cereal Sci. **54**, 224-228 (2011b).

Tarleton, E. Charalambides, M. N, and C. Leppard, "Image-based modelling of binary composites," Comp. Mat Sci. **64**, 183-186 (2012).

Taylor, R. L., K. S. Pister, and G. L. Goudreau, "Thermomechanical analysis of viscoelastic solids," Int. J. Numer. Met. Eng. **2**, 45-59 (1970).

Treloar, L. R. G., *The Physics of Rubber Elasticity* (Clarendon Press, Oxford, 1975).

Underwood, E. E., *Quantitative Stereology* (Addison-Wesley Publishing Company, New York, 1970).

Uthayakumaran, S., M. Newberry, N. Phan-Thien, and R. Tanner, "Small and large strain rheology of wheat gluten," Rheol. Acta **41**, 162-172 (2002).

Vilgis, T. A., "Neutron scattering from a deformed "van der Waals chain"-quasi Gaussian approximation," Colloid Polym. Sci. **270**, 431-436 (1992).

Wang C., S. Dai, and R. I. Tanner, "On the Compressibility of Bread Dough," Korea-Aust. Rheol. J., **18**(3), 127-131 (2006).

Williams, J. G., *Stress Analysis of Polymers* (John Wiley, London, 1980).

Winter, H. H., and F. Chambon, "Analysis of linear viscoelasticity of a cross-linking polymer at the gel point," J. Rheol. **30**, 367-382 (1986).

Winter, H. H., and M. Mours, "Rheology of polymers near liquid-solid transitions," Adv. Polym. Sci. **134**, 165-233 (1997).

List of Figures

FIG. 1. (a) Stress-strain curve of wheat flour dough under uniaxial tension in different regions, and (b) starch and gluten interactions in the different regions ((b)i is reproduced from Amemiya and Menjivar (1992) and (b)iii from Dobraszczyk and Morgenstern (2003)). Stress and strain in 1(a) are calculated through Eqs. (1) and (2).

FIG. 2. Uniaxial compression results of starch at 5/min. Log strain is evaluated through Eq. (2).

FIG. 3. Log strain vs time for cyclic-compression of gluten at 5/min.

FIG. 4. SAOS test results of dough: (a) strain sweep tests in the shear strain range of up to 100 % at 1 Hz, and (b) frequency sweep at 0.1 % shear strain at 0.1-30 Hz.

FIG. 5. Dough test data at 5/min and Lodge rubberlike model fit results under: (a) compression, (b) tension, (c) shear, and (d) Experimental over Lodge model ratio under different modes of deformation.

FIG. 6. Cryo-SEM images of: (a) undeformed dough, (b) undeformed gluten, (c) compressed dough, and (d) stretched dough.

FIG. 7. Gluten test results and calibration of visco-hyperelastic (van der Waals) material model under: (a) compression, (b) tension, (c) shear, (d) cyclic-compression, (e) compression-relaxation, and (f) shear-relaxation. The model is described by Eq. (14) to Eq. (19).

FIG. 8. Starch tests results and calibration of visco-hyperelastic material model with starch tests data under: (a) compression, (b) compression-relaxation at strain of 1, and (c) cyclic-compression.

FIG. 9. Volume fraction measurement of dough: (a) cryo-SEM image of dough, (b) binary image of dough, and (c) a single-particle model of dough.

FIG. 10. Dough tests data at 5/min and calibration of the single-particle model under: (a) compression, (b) tension, and (c) shear.

FIG. 11. Cohesive contact parameters used in the micromechanics model under normal and shear loading.

FIG. 12. Dough tests data and calibration of the single-particle model under: (a) compression, (b) tension, (c) shear, and (d) cyclic-compression.

FIG. 13. Dough shear tests data at 0.5/min and calibration of the single-particle model using lower shear stress initiation value of 0.1 kPa. The other parameters for the single-particle model with damage are the same as in Fig. 11.

FIG. 14. The effect of two different sets of values for the cohesive parameters on global results under uniaxial tension.

FIG. 15. (a) Multi-particle model produced using the image in Fig. 9(b), and (b) comparison results between the single-particle model and the multi-particle model under uniaxial tension mode. The cohesive parameters used are as shown in Fig. 11.

FIG. 16. Comparison results between the 2D single-particle and 3D single-particle models under uniaxial tension mode.